Bull. Mater. Sci., Vol. 18, No. 1, February 1995, pp. 81–91. © Printed in India.

Microstructural features of $Cd_{0.8}Zn_{0.2}Te$ thin films studied by X-ray diffraction and electron microscopy

B SAMANTA, U PAL*, B K SAMANTARAY, T B GHOSH, S L SHARMA and A K CHAUDHURI

Department of Physics and Meteorology, Indian Institute of Technology, Kharagpur 721 302, India

† Universidad Complutense, Departmento Fisica de Materiales, Facultad de Ciencias Fisicas, 28040 Madrid, Spain

Abstract. Thin films of synthesized $Cd_{0.8}Zn_{0.2}Te$ have been deposited on glass substrate at different substrate temperatures. Different microstructural parameters like crystallite size, rms strain, dislocation density, stacking fault probability and stacking fault energy are determined by XRD, SEM, TEM and TED. XRD and XPS have been used to determine the composition. Variations of the microstructural parameters with film thickness and substrate temperature have been studied in order to obtain optimum growth condition for maximum particle size and least microstructural defects. An effort has been made to correlate the experimental results.

Keywords. Thin film; $Cd_{1-x}Zn_xTe$; X-ray diffraction; electron microscopy.

1. Introduction

$Cd_{1-x}Zn_xTe$ is one of the II–VI ternary semiconductor materials whose band gap can be tailored to any value between 1·45 eV and 2·23 eV (Pal *et al* 1989; Saha *et al* 1989). It is a promising material for high efficiency tandem solar cells (Rohatgi *et al* 1989), switching (Patel 1986) and other optoelectronic devices (Dean 1979; Svob and Marfaing 1986). It is also the most suitable substrate material for epitaxial growth of $Hg_{1-x}Cd_xTe$ because both these materials have similar structure, with lattice parameters varying almost linearly with composition (Bruder *et al* 1990).

Several studies have been carried out to find bulk as well as thin film properties of CdTe and ZnTe. However, very little is known about the thin film properties of $Cd_{1-x}Zn_xTe$. The present work aims at the synthesis of $Cd_{0.8}Zn_{0.2}Te$, deposition of thin $Cd_{0.8}Zn_{0.2}Te$ film of different thicknesses at different substrate temperatures and characterization of the deposited films for various microstructural parameters such as crystallite size, microstrain, stacking fault probability and stacking fault energy and dislocation density. These parameters are determined from X-ray diffraction (XRD), scanning electron microscopy (SEM), transmission electron microscopy (TEM) and transmission electron diffraction (TED) studies.

2. Experimental

2.1 *Preparation of the material*

$Cd_{0.8}Zn_{0.2}Te$ was synthesized from its constituent elements (spectroscopically pure) taken in a carbon coated quartz ampoule. The ampoule with the charge was sealed under vacuum ($\approx 10^{-5}$ torr) and suspended in a vertical tantalum furnace at 1123 K

to start the reaction. After 6 h, the temperature was sharply raised to 1433 K (40° above the melting point) (Steininger *et al* 1970) in order to avoid constitutional super cooling effect. After 6 h, the furnace was slowly cooled to room temperature.

From XRD data of the synthesized material, the interplanar spacings (d_{hkl}) were determined. These values lie between those of CdTe (8 F) and ZnTe (8 F) as expected for ternary compound. The notation within the parentheses (as described in the ASTM standard method for assigning phase designation) indicate the Bravis lattice of the materials to be fcc with 8 atoms in each unit cell. Using the Nelson–Riley plot $[1/2(\cos^2\theta/\sin\theta + \cos^2\theta/\theta)$ vs $a]$ the lattice parameter a_0 was calculated. The value of a_0 so obtained was $0{\cdot}6405 \pm 0{\cdot}0005$ nm. Assuming the linearity of the Vegard's law the composition was found to be $Cd_{0{\cdot}80}Zn_{0{\cdot}20}Te$. The composition so obtained was accurate within 10 at%.

The composition of the bulk material was also estimated by electron spectroscopy for chemical analysis (ESCA). X-ray photoelectron spectra (XPS) were recorded by a VG ESCA LAB MK II spectrometer using AlK_α (1486·6 eV) radiation operating at 12 kV, 10 mA. All scans were recorded at 25 eV pass energy at an analyzer chamber pressure of 10^{-9} torr. Before recording the spectra, the specimen was cleaned with Ar^+ ions. For quantitative analysis, the area under each photoelectron peak was estimated after correcting for background. Atomic percentages were obtained using the published sensitivity factors (Wagner *et al* 1981). Because of the uncertainties of the sensitivity factors and of the background selection, the quantitative estimates were found to be accurate within 15 at% (Wagner *et al* 1981) within the XPS detection limit of ≈ 5 nm from the surface. Under the instrumental conditions employed, the energy resolution of the spectrometer was 0·92 eV. For the analysis, the $Cd(^3d_{5/2})$, $Zn(^2p_{3/2})$ and $Te(^3d_{5/2})$ photoelectron peaks were taken into consideration. The peaks were identified by the electron binding energy position of the pure elements. The binding energy of carbon 1*s* peak at 285 eV was taken as the energy reference (Seah 1983). Composition of the bulk material was thus determined to be $Cd_{0{\cdot}76}Zn_{0{\cdot}24}Te$.

2.2 *Thin film deposition*

Thin films of different thicknesses were deposited on properly cleaned glass substrates at different temperatures by vacuum (10^{-5} torr) evaporation of the synthesized material from a tantalum boat. The rate of deposition was always maintained at about 60 nm/min. The film thicknesses were measured by a Taylor–Hobson Form Talysurf.

2.3 *X-ray line profile analyses*

XRD patterns of various films were obtained by a Philips X-ray diffractometer (PW1729) using monochromatic CuK_α radiation. Ni filter was used for obtaining monochromatic CuK_α radiation. The XRD patterns showed that the films had preferred (111) orientation. The peak heights due to other planes were considerably smaller than those of the bulk sample. The values of the lattice parameter as obtained from XRD data of different films are shown in table 1.

The crystallite size and rms strain values for the (111) reflections were calculated by variance analysis (Mitra 1964). This method is sensitive to the variation near the

Table 1. Microstructural parameters for $Cd_{0.8}Zn_{0.2}Te$ thin films deposited at different substrate temperatures (T_s).

Subs. temp T_s (K)	Film thickness (nm)	Lattice constant (nm)	Particle size (nm)	rms strain (10^{-3})	Stacking fault prob.	Stacking fault energy (mJ/m^2)	Dislocation density (lines/m^2) 10^{14}
	240	0·6410	33	8·2	0·061	8·81	50·7
	320	0·6418	52	7·6	0·052	8·89	29·1
	460	0·6412	77	7·0	0·044	8·91	18·6
300	610	0·6404	117	6·4	0·036	9·09	11·2
	710	0·6408	152	6·1	0·031	9·60	8·2
	800	0·6410	119	6·8	0·039	9·48	11·7
375	980	0·6410	150	6·9	0·037	10·29	9·4
475	800	0·6416	165	4·7	0·026	6·80	5·8
575	850	0·6410	174	5·0	0·026	7·69	5·8

tails of the peaks, so a careful adjustment of the background was carried out (Mitra and Misra 1966). Assuming that the broadening of the line profile is due to the crystallite size and strain only, the variance is given by (Klug and Alexander 1974):

$$W_{2\theta} = \frac{S\lambda\sigma}{2\pi^2 p \cos\theta} + 4\tan^2\theta\langle e^2\rangle, \tag{1}$$

where $W_{2\theta}$ is the variance calculated in 2θ scale, p the particle size, σ the angular range over which the intensity is appreciable, $\langle e^2\rangle$ the mean squared lattice strain, λ the wavelength of the radiation used, θ the Bragg angle and S the Scherrer constant whose value for the cubic constant can be taken to be unity. For calculating the variance a suitable background was drawn. The angular range of this profile in radians was the first value (maximum) of σ. This range was then divided into several divisions. A new background line was then drawn by reducing the profile by one division from each end. This new range was the next σ and corresponding $W_{2\theta}$ was calculated. Thus several σ and corresponding $W_{2\vartheta}$ were computed. The error in the range values lies within $\pm 3{\cdot}492 \times 10^{-4}$ radian. The particle size (p) and the rms strain $\langle e^2\rangle^{1/2}$ can be calculated from the slope and intercept of the straight line respectively. A typical variance ($W_{2\theta}$) vs range (σ) plot is shown in figure 1.

The lower limits of dislocation density (ρ) for the films were calculated using the method suggested by Williamson and Smallman (1956).

Stacking fault probability (α) is the fraction of layers undergoing stacking sequence faults and hence one fault is expected in $1/\alpha$ layers. Stacking fault probability α is determined by Fourier analysis of the X-ray line profile using the formula (Warren 1969):

$$\frac{1}{D_{(\text{eff, }111)}} = \frac{1}{D} + (\sqrt{3}/4)\frac{(1{\cdot}5\alpha + \beta)}{a}. \tag{2}$$

Here $D_{(\text{eff, }111)}$ is the average crystal dimension obtained from the intercept of the initial slope on the axis of abscissae of A_L^S vs L plot, A_L^S being the size coefficient and

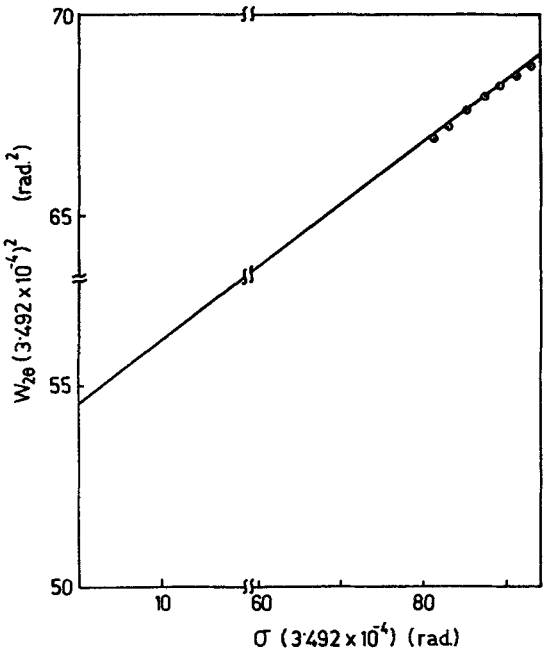

Figure 1. Variance ($W_{2\theta}$) vs angular range (σ) plot for $Cd_{0.8}Zn_{0.2}Te$ thin films having thickness 710 nm deposited at 300 K.

L being the real distance along the columns of cells perpendicular to reflecting planes. D is the true particle size, a the lattice parameter and β the twin fault probability which is assumed to be zero in this case.

Occurrence of stacking faults also gives rise to shift in the peak positions of the samples with respect to the ideal positions of a fault free sample in the XRD pattern. Warren and Warekois (1955) have given a relation connecting α with the shift $\Delta(2\theta)$:

$$\alpha = \frac{2\pi^2}{45\sqrt{3}\tan\theta_{111}}\Delta(2\theta^0_{111}). \tag{3}$$

The value of α determined by Fourier coefficient technique is used here to calculate the $\Delta(2\theta^0_{111})$ value in (3). Thus we obtained the corrected peak position ($2\theta_0$) of the line profile for stacking fault free sample. Taking this $2\theta_0$ as the reference of the profile and after proper correction for geometrical profile, centroids of the profiles were obtained. Then d_{hkl} values were calculated.

From the stacking fault probability, the stacking fault energy can be calculated with the empirical expression suggested by Reed and Schramm (1974).

The surface morphology was studied with a Camscan series II DV electron microscope. SEM photographs of the thin films were taken after etching the upper surface of the films by bromine (1%) methanol vapour in order to reveal the grains properly. SEM photographs for few typical films are shown in figures 2a–c.

TEM and TED patterns of films deposited at different substrate temperatures were obtained with the help of a JEOL, JEM 200 CX electron microscope using 100 kV electrons. The films having thickness less than 100 nm were etched from the glass

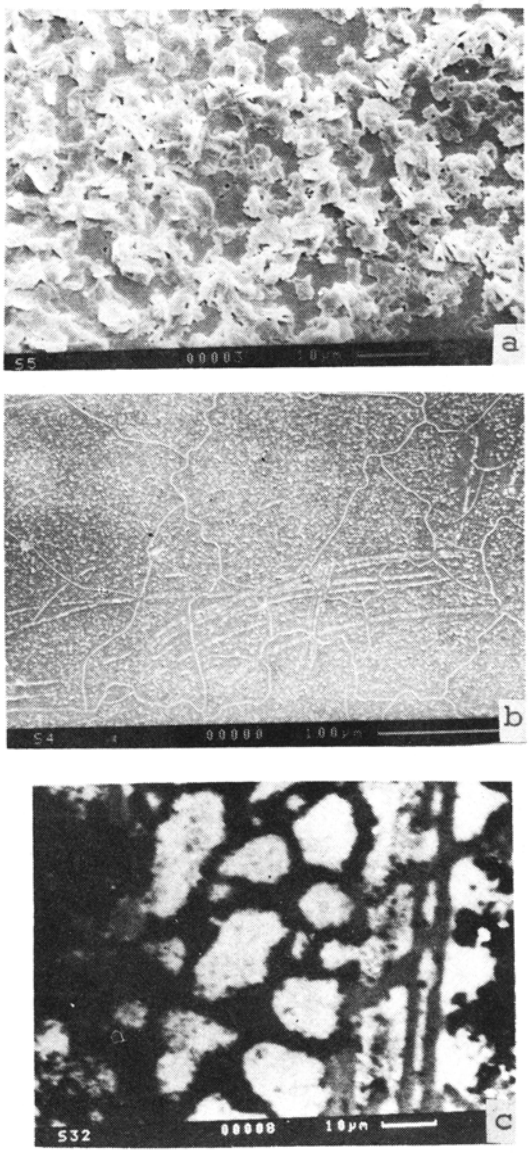

Figure 2. **a.** SEM photograph of thin film having thickness 710 nm deposited at 300 K, **b.** thin film having thickness 240 nm deposited at 300 K and **c.** thin film having thickness 850 nm deposited at 575 K.

substrates using $HNO_3 + HF + H_2O$ (3:2:2) solution and were studied by transmission electron microscope.

3. Results and discussions

XRD pattern of the synthesized material shows peaks corresponding to the cubic phase only. From Nelson–Riley plot, the lattice constant a_0 is found to be 0·6405 nm.

The XRD patterns of the films deposited at different substrate temperatures (300, 375, 475, and 575 K) reveal the preferential growth of the crystallites with (111) planes parallel to the substrate. Peaks due to the planes (220) and (311) are also observed and found to be very weak. No peak corresponding to the hexagonal phase appears in the XRD patterns. In the present investigation, as observed from TEM and TED photographs, hexagonal phase appears with the cubic phase for all the films studied. The appearance of lamellas within the grains in TEM photographs are very clear. It is also clear from TED and TEM studies that the hexagonal phase increased with substrate temperature.

From Nelson–Riley plots for the films, lattice constants a_0 are calculated and tabulated in table 1. XRD analysis does not show much deviation in a_0 or in zinc content (x) values of the $Cd_{1-x}Zn_xTe$ films from those for the bulk material.

From the XRD patterns of the films deposited at room temperature, the crystallite size, rms strain, dislocation density, stacking fault probability and stacking fault energy have been calculated and tabulated in table 1. Variations of crystallite size and rms strain with film thickness are shown in figure 3. It is seen that the crystallite

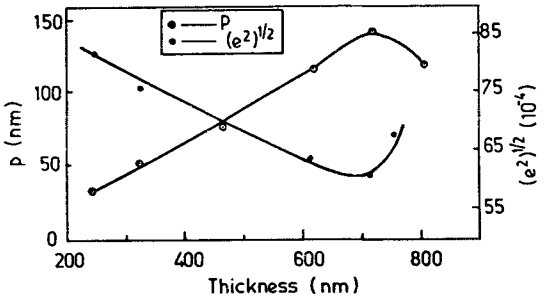

Figure 3. Variations of particle size (p) and rms strain $\langle e^2 \rangle^{1/2}$ with the thickness of the films deposited at 300 K.

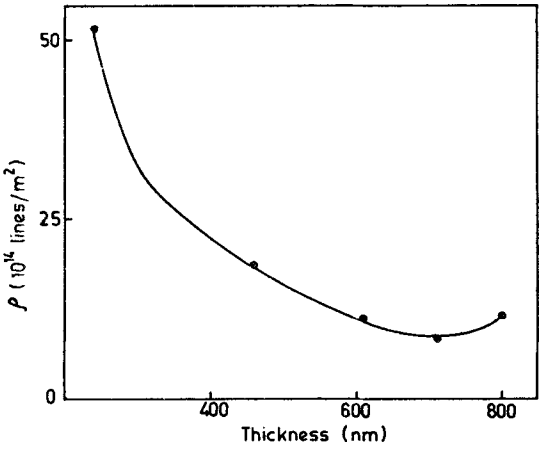

Figure 4. Dislocation density (ρ) vs film thickness for the films deposited at 300 K.

size increases with the film thickness and achieves its maximum value at thickness ≈ 700 nm. This is also seen from the SEM photographs (see figures 2a–b) where the maximum average grain size is found to be ≈ 3000 nm. The rms strain is found to decrease with the film thickness ($\approx 6 \times 10^{-3}$ at thickness ≈ 700 nm).

The variation of dislocation density with film thickness is shown in figure 4. Dislocation density decreases with the film thickness and achieves its minimum value at ≈ 700 nm. Dislocation network can be seen in the SEM photograph of very thin film (figure 2b). Dislocation network is not observed in the SEM photographs for films having thickness > 240 nm. Variations of stacking fault probability and stacking fault energy with film thickness are presented in figure 5. The stacking fault probability decreases and hence stacking fault energy increases up to thickness of 700 nm. With the increase of film thickness particle size increases due to coalescence of small crystals. But for thicker films (> 700 nm) stacking fault probability sharply increases with the increase of thickness. This was also observed for CdTe films by Saha *et al* (1988). The large concentration of stacking faults give rise to the growth of microcrystallites of hexagonal phase which probably inhibits the growth of fcc crystallites. This may be the cause of the optimum film thickness (≈ 700 nm) for particle size and rms strain.

From table 1 it is clear that the particle size increases with the substrate temperature. The increase of grain size with the substrate temperature is also very clear from SEM (figures 2a–c), TEM and TED photographs (figures 6 and 7). Appearance of spotty TED rings at higher substrate temperature (see figure 7b) indicates the increase in crystallite size with increase in substrate temperature.

The d_{hkl} values determined from TED patterns of the films deposited at different substrate temperatures are given in table 2. Hexagonal planes are indicated by hexagonal notations.

The zinc content (x) value obtained from the XPS peak area ratios of the bulk sample is 0·24. The estimated x values for different films are within the range from 0·21 to 0·29. These x values are obtained by normalizing the atomic percent of Zn

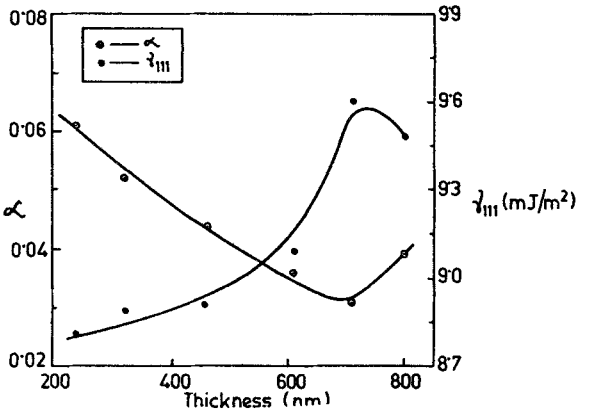

Figure 5. Stacking fault probability (α) and stacking fault energy (γ_{111}) vs thickness of the thin films deposited at 300 K.

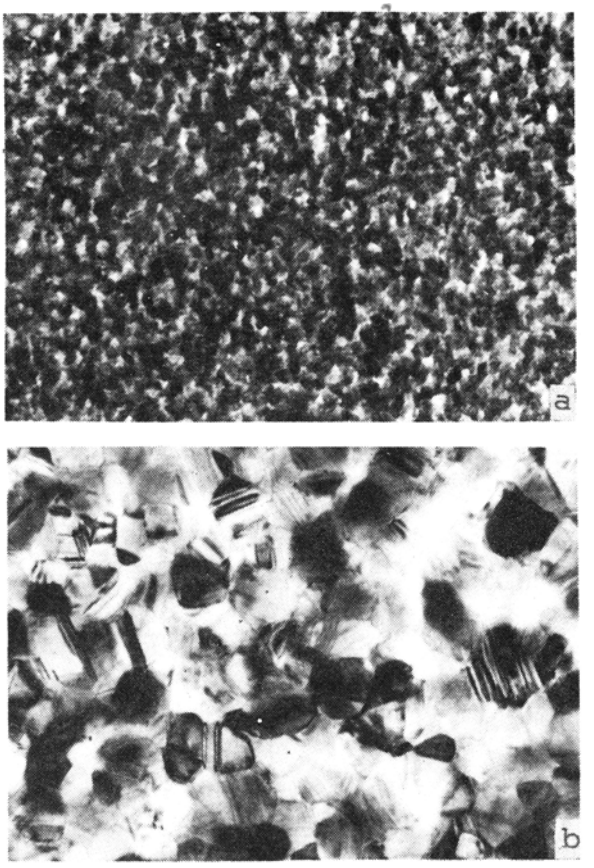

Figure 6. TEM photographs (with magnification $\times 66000$) of $Cd_{0.8}Zn_{0.2}Te$ thin films deposited at (**a**) 300 K and (**b**) 575 K.

and Cd present in the samples. A maximum deviation of nearly 10 at% from the stoichiometric value of Te is observed. However, this is well within the experimental accuracy limit. In table 3, atomic percent of the elements estimated from XPS analyses are given. No systematic variation of the composition with the film thickness or with the substrate temperature is observed. This may be due to the insensitivity of the technique to determine such a small variation. However, for all the films and for the bulk sample, the x values estimated by XPS analyses are higher than the corresponding x values obtained from XRD data.

The rms strain, dislocation density, stacking fault probability and stacking fault energy values decreased with the substrate temperature. Initially the decrease was quite sharp but it became marginal at higher substrate temperatures. This is possibly because of the fact that when the substrate is kept at a higher temperature the dislocations get more thermal energy and have a higher mobility.

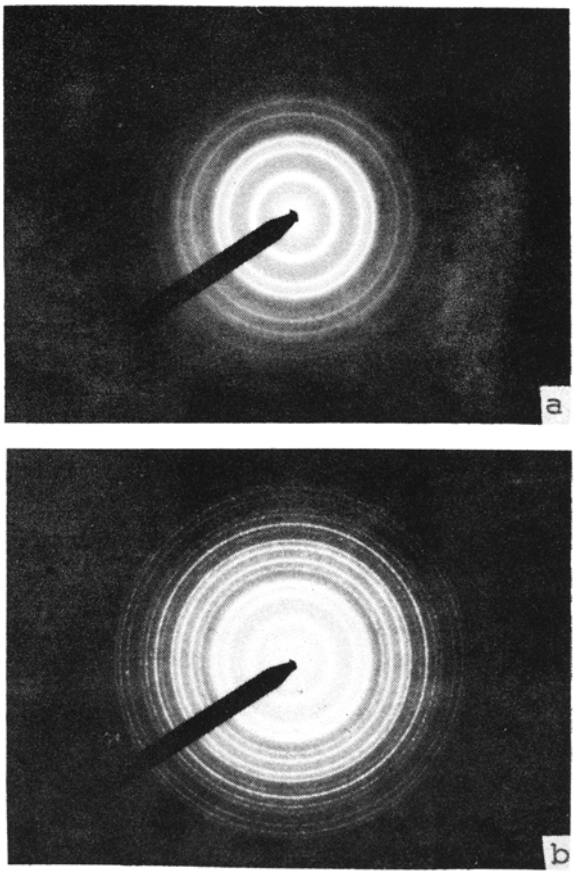

Figure 7. TED photographs of $Cd_{0.8}Zn_{0.2}Te$ thin films deposited at (**a**) 300 K and (**b**) 575 K.

4. Conclusion

Hexagonal phase appears along with the cubic phase even for the $Cd_{0.8}Zn_{0.2}Te$ films deposited at room temperature. The proportion of hexagonal phase increases with the substrate temperature. The stacking fault probability in the films decreases with the thickness causing an increase of stacking fault energy. At higher substrate temperatures particle size becomes larger and stacking fault probability decreases. Therefore we may conclude that for $Cd_{0.8}Zn_{0.2}Te$ thin films least microstructural defects are observed for optimum thickness of ≈ 700 nm and at 575 K substrate temperature. At this temperature films with very large crystallite size and least dislocation density can be obtained. TED also shows single crystal type spots in the diffraction pattern of the film deposited at this temperature.

Table 2. Interplanar spacing values obtained from TED patterns of thin films deposited at different substrate temperatures (T_s).

$T_s = 300$ K		$T_s = 375$ K		$T_s = 475$ K		$T_s = 575$ K	
d_{hkl} (nm)	hkl	d_{hkl} (nm)	hkl	d_{hkl} (nm)	hkl	d_{hkl} (nm)	hkl
0·371	111	0·372	111	0·371	111	0·371	111
0·210	$10\bar{1}3$	0·211	$10\bar{1}3$	0·266	$10\bar{1}2$	0·268	$10\bar{1}2$
0·193	311	0·147	331	0·226	220	0·227	220
0·146	331	0·138	$20\bar{2}4$	0·193	311	0·209	$10\bar{1}3$
0·1227	511	0·1231	511	0·189	$20\bar{2}1$	0·193	311
0·1135	440	0·1137	440	0·159	400	0·189	$20\bar{2}1$
0·1080	531	0·1081	531	0·148	331	0·159	400
0·1010	620	0·1010	620	0·1267	$21\bar{3}3$	0·146	331
		0·0975	533	0·1231	511	0·130	422
		0·0922	444	0·1132	440	0·1229	511
		0·0836	731	0·1082	531	0·1133	440
				0·1015	620	0·1076	531
				0·0977	533	0·1045	$13\bar{4}3$
				0·0897	711	0·1010	620
				0·0858	642	0·0976	533
				0·0832	731	0·0920	444
						0·0894	711
						0·0854	642
						0·0833	731

Table 3. Composition analyses.

Substrate temperature (K)	Film thickness (nm)	Cd atom (%)	Zn atom (%)	Te atom (%)	Value of x obtained from ESCA	Value of x obtained from XRD
	240	38	13	49	0·25	0·19
	320	36	13	51	0·27	0·17
	460	40	14	46	0·26	0·18
300	610	39	13	48	0·25	0·20
	710	40	11	49	0·22	0·19
	800	39	12	49	0·24	0·19
375	980	32	13	55	0·29	0·19
475	800	38	10	52	0·21	0·17
575	850	39	11	50	0·22	0·19

References

Bruder M, Schwarz H–J, Schmitt R, Maier H and Omöler M 1990 *J. Cryst. Growth* **101** 266

Dean P J 1979 *J. Lumin.* **18–19** 755

Klug H P and Alexander L E 1974 *X-ray diffraction procedures for polycrystalline and amorphous materials* (New York: Wiley-Interscience Pub.) p. 661

Mitra G B 1964 *Acta Crystallogr.* **17** 765

Mitra G B and Misra N K 1966 *Br. J. Appl. Phys.* **17** 1319

Pal U, Saha S, Chaudhuri A K, Rao V V and Banerjee H D 1989 *J. Phys. D: Appl. Phys.* **22** 965
Patel N G 1986 *J. Mater. Sci.* **21** 2097
Reed R P and Schramm R E 1974 *J. Appl. Phys.* **45** 4705
Rohatgi A, Ringel S A, Sudharsanan R, Meyers P V, Liu C H and Ramanathan V 1989 *Solar Cells* **27** 219
Saha S, Pal U, Samantaray B K and Chaudhuri A K 1988 *Thin Solid Films* **164** 85
Saha S, Pal U, Chaudhuri A K, Rao V V and Banerjee H D 1989 *Phys. Status Solidi* **114** 721
Seah M P 1983 in *Practical surface analysis* (New York: John Wiley and Sons, Inc.) p. 181
Steininger J, Strauss A J and Brebrick R F 1970 *J. Electrochem.* **117** 1305
Svob L and Marfaing Y 1986 *Solid State Commun.* **58** 343
Wagner C D, Davis L E, Zeller M V, Taylor J A, Raymond R A and Gale W C H 1981 *Surf. Interface Anal.* **3** 211
Warren B E 1969 *X-ray diffraction* (Massachusetts: Addition-Wesley) p. 293
Warren B E and Warekois E P 1955 *Acta Metallogr.* **3** 473
Williamson G N and Smallman R E 1956 *Philos. Mag.* **1** 34